Engineered Science
DOI: https://dx.doi.org/10.30919/es1644

Autonomous Enrichment of Ultra-low Concentration Sb(III) by Gradient P(AA-AM-NH_2-β-CD) Hydrogels Reinforced via Hofmeister Effect

Zihan Han, Yuhan Zhang, Qianyuan Wang, Wenhui Zhang, Kunyan Sui* and Pengfei Qi*

Abstract

Gradient hydrogels offer significant promise for autonomous enrichment of heavy metal ions. However, the instability of the gradient hydrogel induced by high osmotic pressure limits its application, especially for the enrichment of ultra-trace levels of neutral heavy metal species. Here, we designed a gradient hydrogel for autonomous enrichment of ultra-low concentrations of Sb(III) species. The network chain density and gradient structural distribution of the hydrogel were regulated via ion-specific effects. Gradient P(AA-AM-NH2-β-CD)-Na_2SO_4 hydrogel possesses superior mechanical strength, anti-swelling resistance, and built-in electric potential. At an ultra-low concentration of 1 mg/L Sb(III), gradient P(AA-AM-NH2-β-CD) hydrogel exhibits markedly improved Sb(III) enrichment efficiency, which is pH-independent compared to the gradient hydrogel without salt treatment, resulting from the formation of multiple hydrogen bonds. This study demonstrates the potential of Hofmeister effect-reinforced the gradient hydrogels for the autonomous removal of trace heavy metals, also opening new avenues for advanced functional hydrogels.

Keywords: Gradient P(AA-AM-NH2-β-CD) hydrogel; Hofmeister effect; Autonomous enrichment of Sb(III); Hydrogen bond.
Received: 21 June 2025; Revised: 19 July 2025; Accepted: 21 July 2025.
Article type: Research article.

1. Introduction

Heavy metals are ubiquitous environmental pollutants that bioaccumulate and pose severe risks to ecosystems and human health, they are typically non-biodegradable and can be highly toxic or carcinogenic even at trace levels.[1–3] Traditional wastewater treatment techniques such as flocculation and sedimentation, membrane adsorption, *etc*. are widely used in the treatment of heavy metal ions.[4–6] However, most of these methods have drawbacks such as low efficiency and high energy consumption. Comparing to the traditional removal methods, the autonomous deep removal of heavy metal ions has attracted attention as it does not require external stimuli to be triggered. For ultra-low concentration heavy metal ions, due to the limitations of low concentration gradients, autonomous removal of trace heavy metal ions still faces big challenges.[7–9]

Recently, several self-driven methods are available for effective removal of heavy metal pollutants from water, including micro/nanomotor, triboelectric nanogenerator, and the materials with chemical gradient.[10-13] However, micro/nanomotorsare hard to remove from water using conventional methods,[14–16] potentially leading tosecondary pollution. Triboelectric nanogenerators may suffer from limited current output, flow-rate dependence, and instability in fluctuating environments.[17–19] Among them, the ion permeability of hydrogels has gained wide attention, particularly for hydrogels with chemical gradients. For example, E-jet printing can create micrometer-scale potential chemical wells in hydrogel films for directional transport and enrichment of specific molecules.[20] However, this requires specific analyte-substrate interactions, which limits its applicability. Gradient gel materials can also be used.[21-26] For instance, dynamic ion waves can drive the transport and enrichment of hydrophilic molecules in hydrogels.[27] Locally adding ions to a hydrogel can form dynamic chemical gradients to propel hydrophilic molecules. But in practical applications, introducing specific ion solutions to create dynamic gradients may pose challenges in compatibility and stability. We previously reported the self - driven removal of anionic heavy metals such as As (V) and Sb (V) based on the gradient hydrogel, and further improved the removal efficiency based on the built-in potential and interfacial

Qingdao University, No.308 Ningxia Road, Qingdao, 266071, China
**Email:* sky@qdu.edu.cn (K. Sui); pengfei@uni-bremen.de (P. Qi)

potential,[28,29] and for neutral trace heavy metal ions, self-driven removal can be realized based on hydrogen bonding and so on.[30] However, the hydrogels containing a large number of charged and hydrophilic groups hydrogels exhibit high swelling properties due to their high osmotic pressure, thereby weakening the gradient structural distribution and mechanical properties of the hydrogel.[31,32] Recent studies have demonstrated that ion-specific effects can be used to modulate the polymer network density and mechanical properties of hydrogels.[33–37] For example, the salting-out effect triggered by sodium sulfate solution enhances the mechanical properties of polyvinyl alcohol/gelatin double-network hydrogels, endowing them with excellent mechanical properties.[38] Also, the Young's modulus of the hydrogels could be enhanced from 10^{-2} MPa to 10^{3} MPa via salt solution regulation.[39] And by changing the types of coexisting ions, the phase separation of common polyacrylic acid single-network hydrogels is induced, which greatly boosts their strength and toughness.[40] Therefore, we propose to modulate the gradient structural distribution and network density of hydrogels via ion-specific effects.

In this work, we designed a gradient poly(acrylic acid–acrylamide–aminated β-cyclodextrin) (P(AA-AM-NH_2-β-CD)) hydrogel via single-sided UV polymerization method, and regulated the network density and gradient structure distribution via Hofmeister effect. We systematically optimize its composition (monomer content and ratio) to maximize built-in potential and minimize swelling. Crucially, the build-in potential of gradient P(AA-AM-NH_2-β-CD) hydrogel and network chain density was enhanced via treatment of Na_2SO_4, as well as the viscoelasticity and mechanical properties of the hydrogels. Gradient P(AA-AM-NH_2-β-CD) hydrogel treated by Na_2SO_4 solution achieves markedly enhanced Sb(III) enrichment efficiency independent of pH values. This study provides a promising strategy for the autonomous enrichment of trace heavy-metal ions via gradient P(AA-AM-NH_2-β-CD) hydrogels enhanced by ion-specific effect.

2. Experiment

2.1 Materials

β-Cyclodextrin (β-CD), epichlorohydrin (ECH), acrylic acid (AA), acrylamide (AM), N,N′-methylenebisacrylamide (MBAA, cross-linking agent), and 2-hydroxy-4′-(2-hydroxyethoxy)-2-methylpropiophenone (HMEA, photo-initiator, 98%) were acquired from Shanghai Macklin Biochemical Co., Ltd. Sodium sulfate (Na_2SO_4), copper sulfate ($CuSO_4$), magnesium sulfate ($MgSO_4$), ammonium sulfate ($(NH_4)_2SO_4$), sodium chloride (NaCl), sodium iodide (NaI), sodium nitrate ($NaNO_3$), and sodium acetate (CH_3COONa) were purchased from Sinopharm Chemical Reagent Co., Ltd. Antimony potassium tartrate ($K(SbO)C_4H_4O_6 \cdot 3H_2O$) was purchased from Aladdin Reagent Co., Ltd. Ammonium hydroxide (1% aqueous solution) was purchased from Shanghai Yuanye Bio-Technology Co., Ltd. UV absorber (2-(2'-hydroxy-3'-tert-butyl–5'-methylphenyl)-5-chlorobenzotriazole) was purchased from Huaen Rubber & Plastic New Material Co., Ltd. Except for ammonium hydroxide and HMEA, all chemicals were of 99% purity. Ultrapure water (18.25 MΩ·cm) was used throughout the experiments.

2.2 Fabrication of gradient P(AA-AM-NH_2-β-CD) hydrogels

NH_2-β-CD was synthesized following a modified literature procedure.[30] Briefly, 8.1 g of β-cyclodextrin (β-CD) and 6.7 g of potassium hydroxide were dissolved in 70 mL of deionized water in a 250 mL three-necked round-bottom flask, maintained at 50 °C under continuous stirring. After dissolving, 3.4 g of 25 wt% ammonium hydroxide and 10.2 g of ECH were sequentially added. The reaction was conducted at 60 °C for 1 hour. After completion of the reaction, the reaction mixture was cooled to room temperature and acidified to pH 5–6 using sulfuric acid. Subsequently, 150 mL of ethanol was added to precipitate the crude product. The precipitate was purified via neutral alumina column chromatography using 60% (v/v) aqueous ethanol as the eluent. The collected solutions were concentrated to approximately 30 mL, followed by the addition of excess anhydrous methanol. The resulting solid was filtered and vacuum-dried to yield NH_2-β-CD.

1.655 g of acrylamide (AM), 5.037 g of NH_2-β-CD, 0.03 g of N,N'-methylenebisacrylamide (MBAA), 0.09 g of 2-hydroxy-4′-(2-hydroxyethoxy)-2-methylpropiophenone (HMEA), and 0.03 wt% of a UV absorber were dissolved in 30 mL of deionized water under stirring. Subsequently, 5.038 g of acrylic acid (AA) was added, and the mixture was sonicated for 5 minutes to ensure homogeneity and to remove dissolved gases, forming the precursor solution. This solution was injected into a custom-made reaction cell composed of two 10 mm × 10 mm × 3 mm glass plates separated by a 3 mm silicone spacer. The precursor was then polymerized under UV irradiation (365 nm) for 6 hours. The UV source consisted of a 28.5 cm long quartz lamp with an emission wavelength of 365 nm and a total power output of 8 W. The vertical distance between the lamp and the reaction cell was maintained at 3 cm. The homogeneous P(AA-AM-NH_2-β-CD) hydrogel was synthesized following the same procedure, without UV absorber. The polymerization was also carried out under UV irradiation (365 nm) for 6 hours to ensure complete copolymerization.

2.3 Batch experiments

To investigate the Hofmeister effect on gradient P(AA-AM-NH_2-β-CD) hydrogels, samples were immersed in 1.5 M salt solutions for 24 hours at room temperature. The anion series included Na_2SO_4, CH_3COONa, $NaNO_3$, NaCl, and NaI, while the cation series comprised Na_2SO_4, $(NH_4)_2SO_4$, $CuSO_4$, and $MgSO_4$. The gradient hydrogels were immersed in Na_2SO_4 solutions with varying concentrations (0.5, 1.0, 1.5, and 2.0 M) under identical conditions. After treatment, all hydrogels were

thoroughly rinsed with ultrapure water to remove residual salts prior to further analysis.

To investigate the autonomous enrichment behavior of Sb(III), 2.0 g of gradient hydrogel was added to 40 mL of Sb(III) solution at an initial concentration of 1 mg/L and pH 6.0, followed by shaking at 25 °C for 24 h. After enrichment, the supernatant was filtered through a 0.45 μm membrane, and the residual Sb(III) concentration was determined using inductively coupled plasma optical emission spectrometry (ICP-OES). The effects of solid content and monomer molar ratio on the enrichment efficiency of Sb(III) were firstly studied. And then the autonomous enrichment of Sb(III) at different initial Sb(III) concentration ranging from 1 to 10 mg/L was investigated. For kinetic studies, aliquots were withdrawn at specific time intervals, ranging from 5 minutes to 24 hours. The influence of pH was studied by immersing 2.0 g of gradient hydrogels in 40 mL of Sb(III) solution with pH adjusted to 3–11. To assess the reusability of the gradient hydrogel for Sb(III) enrichment, 2.0 g of gradient P(AA-AM-NH_2-β-CD)-Na_2SO_4 hydrogel was immersed in 40 mL of Sb(III) solution (1 mg/L, pH 6.0) for 24 hours. After enrichment of Sb(III), the gradient hydrogels were regenerated using 0.1 M HCl solution. This enrichment–regeneration cycle was repeated for five times.

2.4 Characterization

The built-in potential of the gradient hydrogel was evaluated using a digital source meter (Keithley 2450, Tektronix). The internal gradient structure of the hydrogel was examined on cryo-fractured cross-sections using scanning electron microscopy (SEM, JSM-7800F, JEOL) after rapid freezing in liquid nitrogen and gold sputtering. To visualize the spatial distribution of charged groups within the hydrogel, confocal laser scanning microscopy (CLSM, LSM-800, Zeiss) was employed. Prior to imaging, the hydrogel was stained with a dilute (10^{-2} M) mixed solution of positively charged rhodamine 6G and negatively charged fluorescein sodium. Chemical compositions on the high-density (HD) and low-density (LD) sides of gradient P(AA-AM-NH_2-β-CD) hydrogel were analyzed using X-ray photoelectron spectroscopy (XPS, ESCALAB 250Xi, Thermo Scientific) and Fourier-transform infrared spectroscopy (FT-IR, Nicolet iS50, Thermo Scientific), respectively. Mechanical properties of the hydrogels were tested using a universal testing machine (WDW-5T, China). The rheological behaviors of the gradient hydrogels were analyzed using a rheometer (Phusical MCR 301). Surface charge characteristics were determined by measuring the zeta potential at room temperature with a nanoparticle size–zeta potential analyzer (Nano ZSE, Malvern Panalytical).

3. Results and discussion

3.1 Design of the gradient hydrogels reinforced by Hofmeister effects

Gradient P(AA-AM-NH_2-β-CD) hydrogels were synthesized via a one-pot free radical copolymerization method under unilateral UV irradiation. The monomer mixture comprising AA, AM, and NH_2-β-CD was injected into custom-fabricated molds. Under the induction of unilateral illumination and the presence of a UV absorber, the prepolymer solution on the side exposed to UV illumination was preferentially polymerized, resulting in a higher chain density. And the polymer network density gradually decreased along the thickness direction, resulting in a gradient structure following the attenuation of UV intensity (Fig. S1). CLSM revealed that the positively charged rhodamine 6G dye preferentially accumulated on the HD side, indicating an enriched distribution of negatively charged carboxyl groups (Fig. 1a). In contrast, the negatively charged fluorescein sodium showed a uniform distribution throughout the hydrogel matrix (Fig. 1b), highlighting the selective charge-based interactions within the gradient structure. SEM analysis of the cross-section (Fig. 1c) demonstrated porous architecture with pore sizes gradually increasing from the HD side to the LD side, further confirming the formation of a continuous structural gradient. XPS analysis (Fig. 1d, e and Fig. S2) showed that the atomic percentages of carbon and nitrogen were higher on the HD side compared to the LD side, whereas the oxygen content decreased by 22.15% on the HD side. These differences indicate a greater polymer network density in the irradiated region. FTIR spectra (Fig. 1f) revealed characteristic absorption peaks near 795, 1158, 1645, and 2939 cm^{-1}, corresponding to C–O, C–N, C=O, and N–H stretching vibrations, respectively. These peaks were significantly more intense on the HD side, consistent with a denser chemical network and higher functional group density. Collectively, these results confirm the successful fabrication of a structurally and functionally gradient hydrogel via unilateral UV-induced polymerization.[41]

Due to the abundance of hydrophilic and charged functional groups, gradient P(AA-AM-NH_2-β-CD) hydrogel exhibits significant swelling behavior, accompanied by high osmotic pressure. This internal swelling tendency tends to diminish the built-in potential by weakening the charge gradient. To counteract this effect, ion-specific regulation based on Hofmeister effects was employed to enhance the network density and optimize the gradient distribution of the hydrogel. As shown in Fig. 2a, the built-in potential of the gradient hydrogel exhibited an increasing trend after immersion in different sulfate salts, following the cation sequence: $Na^+ > NH_4^+ > Cu^{2+} > Mg^{2+}$.[42] Similarly, Fig. 2b illustrates the effect of various anions on the built-in potential, in which the enhancement order is: $SO_4^{2-} > Cl^- > NO_3^- > I^- > Ac^-$. Notably, the acetate ion (Ac^-) significantly disrupted the hydrogel's gradient structure due to its strong interaction with polymer chains, resulting in increased swelling and a pronounced reduction in built-in potential. Due to the strong hydration ability of sodium sulfate, the network chain density of the hydrogel was enhanced, resulting in a higher built-in potential. As the concentration of Na_2SO_4 increased, the built-in potential of the gradient hydrogel also increased (Fig. 2c),

indicating enhanced resistance to swelling and improved gradient structure. The hydrogel treated with higher Na_2SO_4 concentrations exhibited reduced swelling ratios (Fig. S3). The strongly hydrated Na^+ and SO_4^{2-} ions could withdraw the free water from the hydrogel, suppressing their swelling and leading to a more compact and ordered network.

Mechanical performance of gradient P(AA-AM-NH_2-β-CD) hydrogels after ion regulation was evaluated through tensile stress–strain tests. As shown in Fig. 2d, the hydrogels treated with different sulfate solutions exhibited distinct mechanical behaviors depending on the cation species. Among them, the hydrogel immersed in Na_2SO_4 displayed the highest tensile strength and elongation at break, indicating superior mechanical integrity. This trend confirms that the enhancement effect of cations on hydrogel mechanical properties generally follows the Hofmeister series: Na^+ > NH_4^+ > Mg^{2+} > Cu^{2+}. Similarly, the mechanical properties of the gradient hydrogels were also improved according to Hofmeister anion sequence (Fig. 2e). In addition, the tensile strength and elongation at break of gradient P(AA-AM-NH_2-β-CD) hydrogels increased with increasing Na_2SO_4 concentration. When the Na_2SO_4 concentration was 2 M, gradient P(AA-AM-NH_2-β-CD)-Na_2SO_4 hydrogel reached the maximum tensile strength (Fig. S4 and Fig. S5), confirming that the strongly hydrated sulfate ions promote the network density and mechanical properties of the hydrogel.

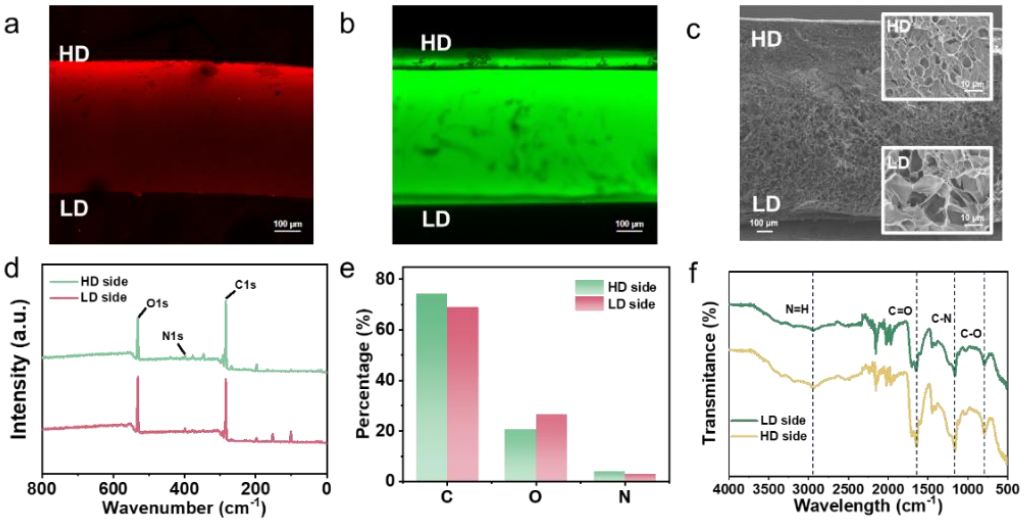

Fig 1: (a) CLSM images after staining with positively charged Rhodamine 6G and (b) negatively charged fluorescein sodium. (c) SEM cross-section of the hydrogel. (d, e) XPS spectra for the HD and LD faces (C1s, O1s and N1s) and (f) FT-IR spectra of gradient P(AA-AM-NH_2-β-CD) hydrogel collected from HD and LD sides.

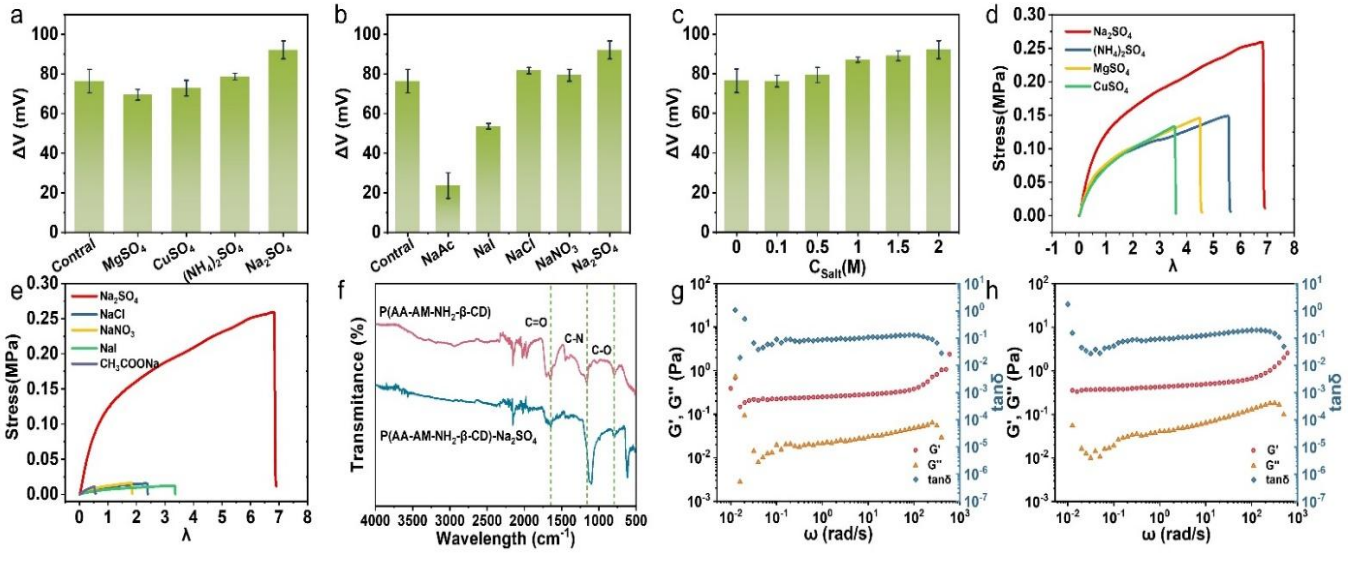

Fig 2: The variation of the built-in potential of gradient P(AA-AM-NH_2-β-CD)-salt hydrogels following treatment (a) cationic sulfates, (b) anionic sodium salts, and (c) different concentrations of Na_2SO_4. Mechanical properties of gradient P(AA-AM-NH_2-β-CD)-salt after different (d) cationic sulfate and (e) anionic sodium salt treatments. (f) FTIR spectra of gradient P(AA-AM-NH_2-β-CD) hydrogel and gradient P(AA-AM-NH_2-β-CD)-Na_2SO_4 hydrogel. Storage modulus G′, loss modulus G″ and loss factor tanδ (G″/G′) of (g) gradient P(AA-AM-NH_2-β-CD) hydrogel and (h) gradient P(AA-AM-NH_2-β-CD)-Na_2SO_4 hydrogel.

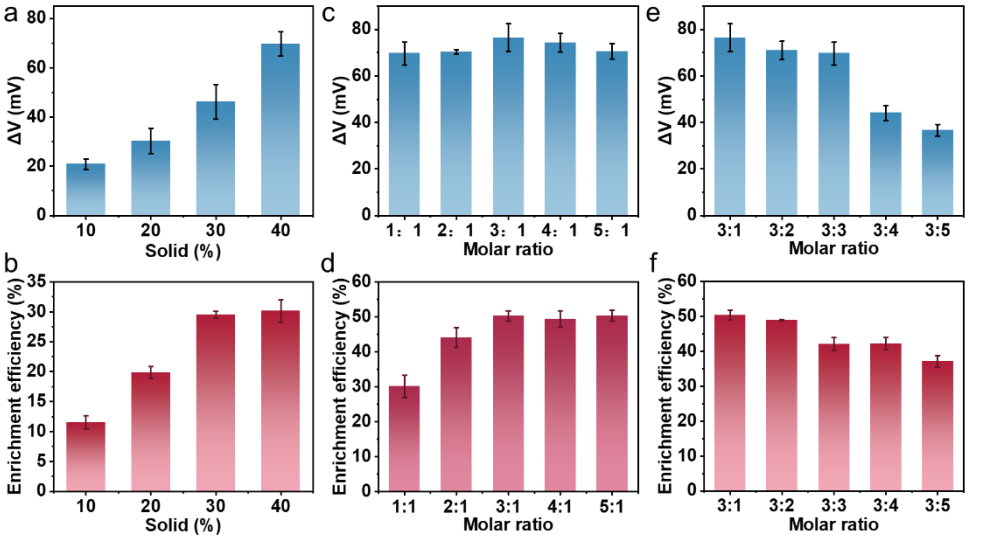

Fig 3: Effects of solid content on (a) built-in potential and (b) Sb(III) enrichment efficiency of gradient P(AA-AM-NH_2-β-CD) hydrogels. Effects of AA:AM molar ratio (with increasing AA content) on (c) built-in potential and (d) Sb(III) enrichment of gradient P(AA-AM-NH_2-β-CD) hydrogels. Effects of AA:AM molar ratio (with increasing AM content) on (e) built-in potential and (f) Sb(III) enrichment of gradient P(AA-AM-NH_2-β-CD) hydrogels.

The chemical environment of the gradient hydrogel after salt solution regulation was thoroughly analyzed. Firstly, FTIR analysis revealed a red shift of the C=O stretching vibration from 1649.25 to 1641.27 cm^{-1} and the C–N stretching vibration from 1158.06 to 1103.65 cm^{-1} (Fig. 2f), indicating the formation of multiple hydrogen bonds between –COOH and $–CONH_2$ groups. In parallel, XPS analysis (Fig. S6) showed that the binding energies of C–N (286.59 eV) and C=O (288.65 eV) increased, and the C=O and C–N peaks exhibited a slight red shift, further confirming the formation of stronger hydrogen bonds. Rheological measurements were further conducted to assess viscoelastic behavior. The gradient P(AA-AM-NH_2-β-CD) hydrogel always present a higher storage modulus (G′) than the loss modulus (G″) (Fig. 2g), indicating its predominantly elastic behavior. After Na_2SO_4 treatment, the G′ of the gradient P(AA-AM-NH_2-β-CD)-Na_2SO_4 hydrogel was enhanced across the entire frequency range, indicating a denser polymer network structure of the hydrogel (Fig. 2h). And the variation of G′ of the gradient hydrogel after treatment with anionic salts also follows the Hofmeister series (Fig. S7). Additionally, the G′ of the gradient hydrogel exhibited varying degrees of enhancement after treatment with different sulfate salts (Fig. S8), indicating that the strongly hydrated sulfate ions play a dominant role in the aggregation of the hydrogel network.

3.2 Optimization of gradient P(AA-AM-NH_2-β-CD) hydrogel fabrication

In order to obtain the optimal gradient distribution, the effect of monomer solid content on the built-in potential of the gradient hydrogel was first investigated. As shown in Fig. 3a, the built-in potential of gradient P(AA-AM-NH_2-β-CD) hydrogel improved when the solid content increased from 10 wt% to 40 wt%. And the enrichment efficiency of Sb(III) also increases with solid content, reaching a plateau at approximately 40 wt% solid content (Fig. 3b). And its swelling ratio correspondingly decreases with the increase of solid content (Fig. S9). Therefore, a solid content of 40% was selected for the preparation of the gradient hydrogels in all subsequent experiments. The effects of monomer molar ratios on the built-in potential and Sb(III) enrichment efficiency of the gradient hydrogel were further investigated. As shown in Fig. 3c, the gradient hydrogels exhibited a slight increase in built-in potential at the AA:AM molar ratio of 3:1. And the Sb(III) enrichment efficiency of the gradient hydrogel increased significantly as the AA:AM molar ratio rises from 1:1 to 3:1, and then approaching equilibrium as the monomer molar ratio increased (Fig. 3d). However, the swelling rate of the gradient hydrogel increases with the increase of the AA monomer proportion due to the enhanced osmotic pressure (Fig. S10). According to the Nernst equation, the concentration difference of carboxyl groups between the upper and lower sides of the gradient hydrogel induces a built-in potential.[43] And the built-in potential of the gradient hydrogel gradually decreases with a decreasing AA:AM molar ratio when the AA content is stable (Fig. 3e). Correspondingly, the Sb(III) enrichment efficiency follows the same trend as the built-in potential of the gradient hydrogel (Fig. 3f). It indicates that the gradient architecture is facilitated for the enrichment of Sb(III). In addition, the gradient hydrogel presents a superior zeta potential and the lowest swelling ratio at an AA:AM molar ratio of 3:1 (Fig. S11). Therefore, a total monomer content of 40 wt% and an AA:AM molar ratio of 3:1 were selected to prepare the gradient P(AA-AM-NH_2-β-CD) hydrogel, which exhibiting the optimal autonomous enrichment towards Sb(III).

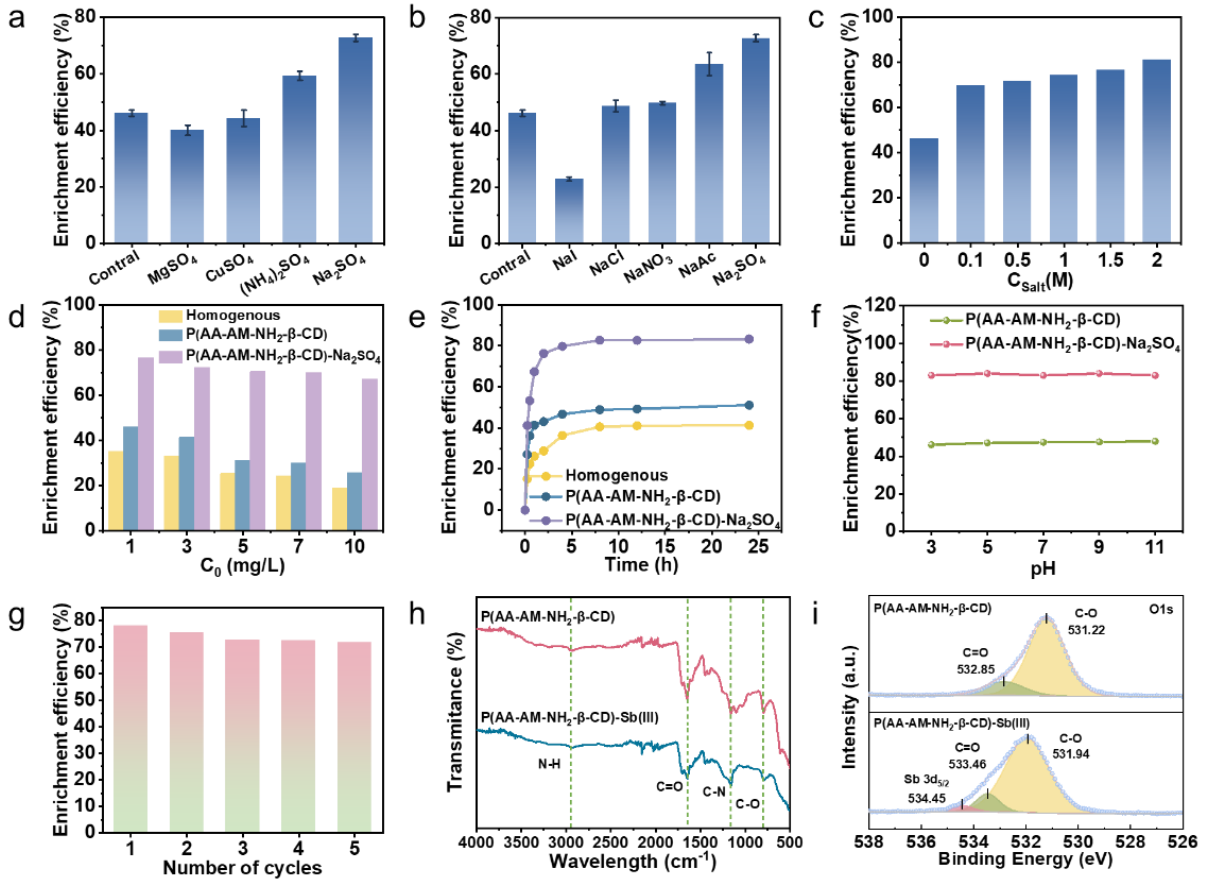

Fig 4: Enrichment of Sb(III) by gradient P(AA-AM-NH_2-β-CD) hydrogels following treatment (a) cationic sulfates, (b) anionic sodium salts, and (c) different concentrations of Na_2SO_4. (d) Enrichment of Sb(III) by three hydrogels at various initial Sb(III) concentrations. (e) Kinetic study on Sb(III) enrichment by three hydrogels. (f) Enrichment of Sb(III) by gradient P(AA-AM-NH_2-β-CD)-Na_2SO_4 hydrogels at different environmental pH levels. (g) Enrichment of Sb(III) by gradient P(AA-AM-NH_2-β-CD)-Na_2SO_4 hydrogels over five cycles. (h) FT-IR spectra comparison of gradient P(AA-AM-NH_2-β-CD)-Na_2SO_4 hydrogels before and after Sb(III) enrichment. (i) XPS spectra comparison of gradient P(AA-AM-NH_2-β-CD)-Na_2SO_4 hydrogels before and after Sb(III) enrichment.

3.3 Autonomous enrichment of Sb(III) by gradient P(AA-AM-NH_2-β-CD) hydrogels regulated via Hofmeister effect

Considering that the network chain density and the gradient distribution of the hydrogel can be enhanced by ion-specific effects, its enrichment performance toward Sb(III) was thoroughly investigated. The enrichment of Sb(III) by gradient P(AA-AM-NH_2-β-CD) hydrogels treated with different sulfate salts and sodium salts was first studied (Fig. 4a and 4b). The results showed that gradient P(AA-AM-NH_2-β-CD)-Na_2SO_4 hydrogel exhibited markedly enhanced enrichment of Sb(III) compared to that of the untreated sample. This improvement can be attributed to the strong hydration ability of SO_4^{2-} ions, which effectively increase the polymer network density and stabilize the gradient distribution. With increasing Na_2SO_4 concentration, the enrichment efficiency of Sb(III) increased and reached a maximum of 76.5% after treatment with 2.0 M Na_2SO_4 (Fig. 4c). The enrichment of Sb(III) at initial concentrations ranging from 1 to 10 mg/L by different types of hydrogels was further studied (Fig. 4d). It was shown that gradient P(AA-AM-NH_2-β-CD)-Na_2SO_4 hydrogel consistently exhibited the highest enrichment efficiency for Sb(III) compared to gradient and homogeneous P(AA-AM-NH_2-β-CD) hydrogels, achieving a high enrichment efficiency of 76.5% for Sb(III) in a 1.0 mg/L solution (pH~6.6). The enrichment kinetics further confirmed this phenomenon. As shown in Fig. 4e, the gradient P(AA-AM-NH_2-β-CD)-Na_2SO_4 hydrogel reached a much higher enrichment efficiency for Sb(III) in a shorter time than the untreated gel. This improvement is mainly attributed to the increased availability of binding sites and the enhanced built-in potential.[29]

Considering that the existing species of Sb(III) is independent of pH values, the effect of pH on the enrichment of Sb(III) by the gradient hydrogels before and after salt treatment was also investigated (Fig. 4f). Gradient P(AA-AM-NH_2-β-CD)-Na_2SO_4 hydrogels exhibited a higher enrichment efficiency towards Sb(III) than the homogeneous hydrogel, independent of pH values. This suggests that the enrichment of Sb(III) is mainly supported by the hydrogen bonds formed between the gradient-distributed hydrogen bond donors and Sb(III) species.

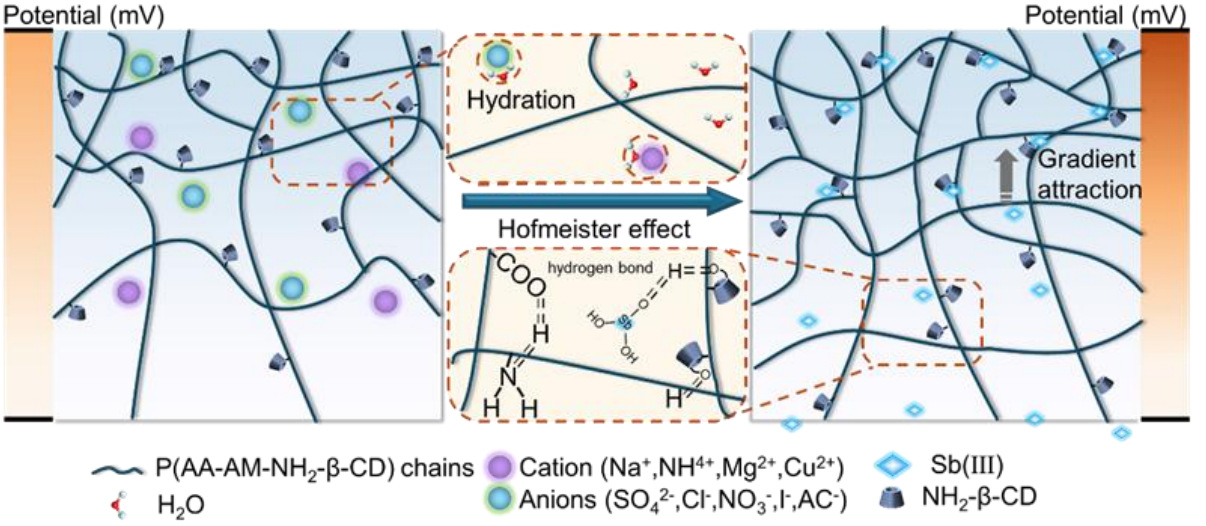

Fig 5: Schematic illustration of the enhanced gradient distribution, network density and Sb(III) enrichment performance of gradient P(AA-AM-NH_2-β-CD) hydrogels regulated by Hofmeister effect.

Importantly, gradient P(AA-AM-NH_2-β-CD)-Na_2SO_4 hydrogel exhibited excellent regeneration capability. As shown in Fig. 4g, after elution with 0.1 M HCl and thorough rinsing, it retained over 70% of its enrichment capacity after five consecutive cycles. The performance remained stable after five cycles, demonstrating good reusability. Subsequently, FTIR and XPS analyses were conducted, to study the interaction mechanism between Sb(III) and the functional groups of the gradient hydrogel. The FTIR spectra (Fig. 4h) of the hydrogel revealed that the characteristic N–H stretching vibration band shifted from 2947 cm^{-1} to a lower wavenumber at 2923 cm^{-1}, while the C=O stretching band moved from 1646 cm^{-1} to 1641 cm^{-1}. XPS analysis (Fig. 4i) identified the Sb $3d_{5/2}$ peak at 534.45 eV, confirming the presence of Sb(III) in gradient P(AA-AM-NH_2-β-CD) hydrogel. Additionally, the C–O and C=O peaks of the carbon spectrum shifted to higher binding energies, consistent with complexation and hydrogen bonding between Sb(III) oxyanions and the hydrogel's functional groups.[44] These red shifts indicate the formation of new hydrogen-bonding interactions between Sb(III) species and the hydrogel's functional groups, suggesting that both –NH_2 and –COOH groups are actively involved in binding Sb(III) through coordination and hydrogen bonding.

A rational mechanism for the autonomous enrichment of Sb(III) by gradient P(AA-AM-NH_2-β-CD) hydrogels regulated via the Hofmeister effect is proposed, as shown in Fig. 5. First, the polymer network chain density and gradient distribution of the gradient hydrogel are enhanced via the Hofmeister effect, where kosmotropic ions (such as SO_4^{2-} and Na^+) induce a salting-out effect by capturing water molecules. These ions effectively remove bound water from the hydrophilic polymer chains, thereby promoting stronger polymer-polymer interactions. This process results in the aggregation of the hydrogel network, increased mechanical stiffness, and enhanced charge density.[45-47] Consequently, the gradient structure is optimized and stabilized, and the formation of hydrogen bonds between Sb(III) and –COOH, –NH_2 groups is promoted, thereby enhancing the autonomous enrichment efficiency of Sb(III) at ultra-low concentration by the hydrogel.

4. Conclusion

In summary, we developed a gradient P(AA-AM-NH_2-β-CD) hydrogel initiated under unilateral UV irradiation and regulated the hydrogel network density and gradient distribution via Hofmeister effect, ultimately improving the autonomous enrichment efficiency of trace Sb(III). The mechanical strength, built-in potential, and the elastic properties of gradient P(AA-AM-NH_2-β-CD) hydrogel were significantly enhanced, following the Hofmeister series of both anions and cations. Sodium sulfate, with its strong hydration ability, promotes network densification and improved gradient distribution within the hydrogel. At a total monomer concentration of 40 wt% and monomer molar ratio of 3:1, the gradient hydrogel presented the optimal enrichment for trace Sb(III). After regulation by Na_2SO_4, gradient P(AA-AM-NH_2-β-CD) hydrogel achieved significantly improved enrichment of Sb(III) at an ultra-low concentration of 1 mg/L, independent of pH. It also has excellent reusability. This enhancement is attributed to the Hofmeister effect, which optimizes the gradient structure of the polymer network and increases the network chain density. As a result, the autonomous enrichment of Sb(III) was significantly enhanced by the formation of hydrogen bonds between Sb(III) species and the gradient-distributed carboxyl and amino groups. This work highlights a simple yet powerful approach to tuning hydrogel properties through ion-specific effects. Kosmotropic ions offer a versatile route to modulate polymer networks, enabling stable and functional gradient materials for applications in environmental remediation and beyond.

Acknowledgments
Zihan Han and Yuhan Zhang contribute equally to this manuscript. The authors acknowledge the financial support from the National Natural Science Foundation of China (No.52472102), and the Natural Science Foundation of Qingdao Municipality (No.24–4–4-zrj-189-jch), and the Program for Taishan Scholar of Shandong Province (No.tstp20231226).

Conflict of Interest
There is no conflict of interest.

Supporting Information
Applicable.

References
[1] T. Münzel, O. Hahad, J. Lelieveld, M. Aschner, M. J. Nieuwenhuijsen, P. J. Landrigan, A. Daiber, Soil and water pollution and cardiovascular disease, *Nature Reviews Cardiology*, 2025, **22**, 71–89, doi: 10.1038/s41569-024-01068-0.
[2] S. Zhang, H. Xu, K. Lu, H. Gao, L. Duan, H. Yu, Q. Li, New insights into pollution source analysis using receptor models: Effects of interaction between heavy metals and DOM on source identification and apportionment in rivers across industrial city, *Journal of Hazardous Materials*, 2025, **484**, 136792, doi: 10.1016/j.jhazmat.2024.136792.
[3] Y. Liu, F. Xu, W. Liu, X. Liu, D. Wang, Characteristics, sources, exposure, and health effects of heavy metals in atmospheric particulate matter, *Current Pollution Reports*, 2025, **11**, 16, doi: 10.1007/s40726-025-00344-y.
[4] S. D. Melvin, F. D. L. Leusch, Removal of trace organic contaminants from domestic wastewater: A meta-analysis comparison of sewage treatment technologies, *Environment International*, 2016, **92-93**, 183–188, doi: 10.1016/j.envint.2016.03.031.
[5] G. İlyasoglu, B. Kose-Mutlu, O. Mutlu-Salmanli, I. Koyuncu, Removal of organic micropollutans by adsorptive membrane, *Chemosphere*, 2022, **302**, 134775, doi: 10.1016/j.chemosphere.2022.134775.
[6] B. A. Mohamed, R. Ruan, M. Bilal, N. A. Khan, M. K. Awasthi, M. A. Amer, L. Leng, M. A. Hamouda, D. N. Vo, J. Li, Co-pyrolysis of sewage sludge and biomass for stabilizing heavy metals and reducing biochar toxicity: A review, *Environmental Chemistry Letters*, 2023, **21** 1231–1250, doi: 10.1007/s10311-022-01542-6.
[7] P. A. Kobielska, A. J. Howarth, O. K. Farha, S. Nayak, Metal–organic frameworks for heavy metal removal from water, *Coordination Chemistry Reviews*, 2018, **358**, 92–107, doi: 10.1016/j.ccr.2017.12.010.
[8] S. Pan, J. Shen, Z. Deng, X. Zhang, B. Pan, Metastable nano-zirconium phosphate inside gel-type ion exchanger for enhanced removal of heavy metals, *Journal of Hazardous Materials*, 2022, **423**, 127158, doi: 10.1016/j.jhazmat.2021.127158.
[9] A. Bashir, L. A. Malik, S. Ahad, T. Manzoor, M. A. Bhat, G. N. Dar, A. H. Pandith, Removal of heavy metal ions from aqueous system by ion-exchange and biosorption methods, *Environmental Chemistry Letters*, 2019, **17**, 729–754, doi: 10.1007/s10311-018-00828-y.
[10] M. Sun, L. Zhang, Y. Li, C. Wang, P. Wang, X. Ren, X. Yi, Recovering Ag^+ with Nano-MOF-303 to form Ag/AgCl/MOF-303 photocatalyst: the role of stored Cl^- ions, *Chinese Chemical Letters*, 2025, **36**, 110035, doi: 10.1016/j.cclet.2024.110035.
[11] L. Zhang, M. Sun, X. Li, M. Liu, H. Chu, C. Wang, P. Wang, X. Yi, Y. Wang, J. Deng, Uranium extraction from radioactive wastewater by NH2-MIL-125 immobilized in a double-network aerogel microsphere, *ACS Sustainable Chemistry & Engineering*, 2025, **13**, 5345–5354, doi: 10.1021/acssuschemeng.5c00543.
[12] S. Chen, R. Ding, B. Li, J. Lu, X. Zhang, A robust aerogel incorporated with phthalocyanine-based porous organic polymers for highly efficient gold extraction, *Separation and Purification Technology*, 2025, **354**, 129451, doi: 10.1016/j.seppur.2024.129451.
[13] X. Pan, J. Ji, N. Zhang, M. Xing, Research progress of graphene-based nanomaterials for the environmental remediation, *Chinese Chemical Letters*, 2020, **31**, 1462–1473, doi: 10.1016/j.cclet.2019.10.002.
[14] H. Huang, J. Li, M. Yuan, H. Yang, Y. Zhao, Y. Ying, S. Wang, Large-scale self-assembly of MOFs colloidosomes for bubble-propelled micromotors and stirring-free environmental remediation, *Angewandte Chemie International Edition*, 2022, **61**, e202211163, doi: 10.1002/ange.202211163.
[15] J. Zhang, Y. Fang, J. Lin, W. Du, Z. Feng, Y. Lin, L. Xu, L. Liu, J. Guan, F. Mou, Generalized and scalable synthesis of manganese dioxide-based tubular micromotors for heavy metal ion removal, *ACS Nano*, 2024, **18**, 29248–29260, doi: 10.1021/acsnano.4c11716.
[16] H. Yang, L. Wang, X. Huang, MOF-based micro/nanomotors (MOFtors): Recent progress and challenges, *Coordination Chemistry Reviews*, 2023, **495**, 215372, doi: 10.1016/j.ccr.2023.215372.
[17] Z. Li, J. Chen, H. Guo, X. Fan, Z. Wen, M. Yeh, C. Yu, X. Cao, Z.L. Wang, Triboelectrification-enabled self-powered detection and removal of heavy metal ions in wastewater, *Advanced Materials*, 2016, **28**, 2983–2991, doi: 10.1002/adma.201504356.
[18] X. Sun, L. Dong, J. Liu, T. Hou, Y. Li, L. Wang, X. Xu, S. Chen, Regulating contact electrification and charge retention capability with metal–organic frameworks in triboelectric nanogenerator for self-powered sewage treatment, *Advanced Functional Materials*, 2025, **35**, 2422803, doi: 10.1002/adfm.202422803.
[19] F. Dong, Z. Pang, S. Yang, Q. Lin, S. Song, C. Li, X. Ma, S. Nie, Improving wastewater treatment by triboelectric-photo/electric coupling effect, *ACS Nano*, 2022, **16**, 3449–3475, doi: 10.1021/acsnano.1c10755.
[20] S. Zhang, S.J. Kieffer, C. Zhang, A.G. Alleyne, P.V. Braun, Directed molecular collection by e-jet printed microscale chemical potential wells in hydrogel films, *Advanced Materials*, 2018, **30**, 1803140, doi: 10.1002/adma.201803140.
[21] A. Dey, M. Ramoni, N. Yodo, A survey on fused filament

fabrication to produce functionally gradient materials, *Materials*, 2024, **17**, 3675, doi: 10.3390/ma17153675.
[22] A. Pragya, T. K. Ghosh, Soft functionally gradient materials and structures–natural and manmade: a review, *Advanced Materials*, 2023, **35**, 2300912, doi: 10.1002/adma.202300912.
[23] A. Perl, A. Gomez-Casado, D. Thompson, H. H. Dam, P. Jonkheijm, D. N. Reinhoudt, J. Huskens, Gradient-driven motion of multivalent ligand molecules along a surface functionalized with multiple receptors, *Nature Chemistry*, 2011, **3**, 317–322, doi: 10.1038/nchem.1005.
[24] C. Xu, N. Sun, H. Li, X. Han, A. Zhang, P. Sun, Stimuli-responsive vesicles and hydrogels formed by a single-tailed dynamic covalent surfactant in aqueous solutions, *Molecules*, 2024, **29**, 4984, doi: 10.3390/molecules29214984.
[25] S. Chen, R. Ding, B. Li, J. Lu, X. Zhang, A robust aerogel incorporated with phthalocyanine-based porous organic polymers for highly efficient gold extraction, *Separation and Purification Technology*, 2025, **354**, 129451, doi: 10.1016/j.seppur.2024.129451.
[26] A. Abdurahman, J. Wang, Y. Zhao, P. Li, L. Shen, Q. Peng, A highly stable organic luminescent diradical, *Angewandte Chemie International Edition*, 2023, **62**, e202300772, doi: 10.1002/anie.202300772.
[27] T. Tsai, M. A. Ali, Z. Jiang, P. V. Braun, Dynamic gradient directed molecular transport and concentration in hydrogel films, *Angewandte Chemie International Edition*, 2017, **56**, 5001–5006, doi: 10.1002/anie.201700166.
[28] S. Qi, M. Lin, P. Qi, J. Shi, G. Song, W. Fan, K. Sui, C. Gao, Interfacial and build-in electric fields rooting in gradient polyelectrolyte hydrogel boosted heavy metal removal, *Chemical Engineering Journal*, 2022, **444**, 136541, doi: 10.1016/j.cej.2022.136541.
[29] S. Qi, Y. Zhang, J. Shi, Y. Wang, J. Gao, W. Fan, K. Sui, P. Qi, Autonomous enrichment and deep removal of heavy metals by salt-tolerant gradient polyelectrolyte hydrogels, *Chemical Engineering Journal*, 2023, **472**, 145158, doi: 10.1016/j.cej.2023.145158.
[30] Y. Zhang, H. Wang, Z. Song, C. Wang, J. Hou, K. Sui, P. Qi, Directed selective transport and enrichment of micropollutants by gradient P(AA-AM-NH_2-β-CD) hydrogels, *Journal of Hazardous Materials*, 2025, **486**, 136929, doi: 10.1016/j.jhazmat.2024.136929.
[31] L. Wang, H. Hemmatpour, P. Rudolf, D. Gerlach, G. J. Euverink, F. Picchioni, Swollen hydrogels with strong mechanical characteristics: A superior adsorbent for the sustainable removal of diclofenac sodium, *Journal of Colloid and Interface Science*, 2025, **686**, 754–763, doi: 10.1016/j.jcis.2025.02.004.
[32] H. Yu, S. Zheng, L. Fang, Z. Ying, M. Du, J. Wang, K. Ren, Z. Wu, Q. Zheng, Reversibly transforming a highly swollen polyelectrolyte hydrogel to an extremely tough one and its application as a tubular grasper, *Advanced Materials*, 2020, **32**, 2005171, doi: 10.1002/adma.202005171.
[33] M. Hua, S. Wu, Y. Ma, Y. Zhao, Z. Chen, I. Frenkel, J. Strzalka, H. Zhou, X. Zhu, X. He, Strong tough hydrogels via the synergy of freeze-casting and salting out, *Nature*, 2021, **590**, 594–599, doi: 10.1038/s41586-021-03212-z.
[34] S. Wu, M. Hua, Y. Alsaid, Y. Du, Y. Ma, Y. Zhao, C. Lo, C. Wang, D. Wu, B. Yao, J. Strzalka, H. Zhou, X. Zhu, X. He, Poly(vinyl alcohol) hydrogels with broad-range tunable mechanical properties via the Hofmeister effect, *Advanced Materials*, 2021, **33**, 2007829, doi: 10.1002/adma.202007829.
[35] L. Xiang, D. Pan, J. Lei, N. AlMasoud, T. S. Alomar, I. G. Issaulu, Y. Wang, Z. M. El-Bahy, C. Liu, Z. Guo, S. Ainur, Z. Toktarbay, Sodium alginate aerogel derived SiC@Co-C 3D network enhances electromagnetic wave absorption and thermal conductivity of PDMS based composite, *International Journal of Biological Macromolecules*, 2025, **306**, 141539, doi: 10.1016/j.ijbiomac.2025.141539.
[36] F. Zhu, S. Feng, Z. Wang, Z. Zuo, S. Zhu, W. Yu, Y. Ye, M. An, J. Qian, Z. Wu, Q. Zheng, Co-Ion specific effect aided phase separation in polyelectrolyte hydrogels toward extreme strengthening and toughening, *Macromolecules*, 2023, **56**, 5881–5890, doi: 10.1021/acs.macromol.2c02583.
[37] R. Guo, Y. Bao, X. Zheng, W. Zhang, C. Liu, J. Chen, J. Xu, L. Wang, J. Ma, Hofmeister effect assisted dual-dynamic-bond cross-linked organohydrogels with enhanced ionic conductivity and balanced mechanical properties for flexible sensors, *Advanced Functional Materials*, 2023, **33**, 2213283, doi: 10.1002/adfm.202213283.
[38] Y. Zhang, Y. Wang, Y. Bao, B. Lin, G. Cheng, N. Yuan, J. Ding, Multifunctional PVA/gelatin DN hydrogels with strong mechanical properties enhanced by Hofmeister effect, *Colloids and Surfaces A*, 2024, **691**, 133833, doi: 10.1016/j.colsurfa.2024.133833.
[39] Y. Jin, S. Lu, X. Chen, Q. Fang, X. Guan, L. Qin, C. Chen, C. Zhao, Time-salt type superposition and salt processing of poly(methacrylamide) hydrogel based on Hofmeister Series, *Macromolecules*, 2024, **57**, 2746–2755, doi: 10.1021/acs.macromol.3c02395.
[40] F. Zhu, S. Feng, Z. Wang, Z. Zuo, S. Zhu, W. Yu, Y. Ye, M. An, J. Qian, Z. Wu, Q. Zheng, Co-ion specific effect aided phase separation in polyelectrolyte hydrogels toward extreme strengthening and toughening, *Macromolecules*, 2023, **56**, 5881–5890, doi: 10.1021/acs.macromol.2c02583.
[41] N. Zinkovska, J. Smilek, M. Pekar, Gradient P(AA-AM-NH_2-β-CD) hydrogels—the state of the art in preparation methods, *Polymers*, 2020, **12**, 966, doi: 10.3390/polym12040966.
[42] J. Gaburjakova, M. Gaburjakova, The cardiac ryanodine receptor provides a suitable pathway for the rapid transport of zinc (Zn^{2+}), *Cells*, 2022, **11**, 868, doi: 10.3390/cells11050868.
[43] H. Wang, M. Du, H. Jiang, R. Zhou, Y. Wang, K. Sui, W. Fan, Gradient p-polyanion/n-polycation heterojunction endows ionic diodes with vastly boosted output voltage, power density and sensitivity, *Advanced Functional Materials*, 2024, **34**, 2407639, doi: 10.1002/adfm.202407639.
[44] H. Zeng, Y. Zeng, H. Xu, S. Sun, J. Zhang, D. Li, Sb(III) Removal by granular adsorbent synthesized with iron-containing water treatment residuals and chitosan, *Polymers*, 2024, **16**, 3214, doi: 10.3390/polym16223214.

[45] W. Wei, Hofmeister effects shine in nanoscience, *Advanced Science*, 2023, **10**, 2302057, doi: 10.1002/advs.202302057.
[46] C. Zeng, P. Wu, J. Guo, N. Zhao, C. Ke, G. Liu, F. Zhou, W. Liu, Synergy of Hofmeister effect and ligand crosslinking enabled the facile fabrication of super-strong, pre-stretching-enhanced gelatin-based hydrogels, *Soft Matter*, 2022, **18**, 8675–8686, doi: 10.1039/D2SM01158A.
[47] G. Cao, L. Zhao, X. Ji, Y. Peng, M. Yu, X. Wang, X. Li, F. Ran, "Salting out" in Hofmeister effect enhancing mechanical and electrochemical performance of amide-based hydrogel electrolytes for flexible zinc-ion battery, *Small*, 2023, **19**, 2207610, doi: 10.1002/smll.202207610.